Journal of Research of the National Bureau of Standards—D. Radio Propagation
Vol. 63D, No. 2, September–October 1959

Diffraction of Electromagnetic Waves by Smooth Obstacles for Grazing Angles [1]

James R. Wait and Alyce M. Conda

(March 19, 1959)

The diffraction of electromagnetic waves by a convex cylindrical surface is considered. Attention is confined primarily to the region near the light-shadow boundary. The complex-integral representation for the field is utilized to obtain a correction to the Kirchhoff theory. Numerical results are presented which illustrate the influence of surface curvature and polarization on the diffraction pattern. Good agreement with the experimental results of Bachynski and Neugebauer is obtained. The effect of finite conductivity is also considered.

1. Introduction

The Kirchhoff theory of diffraction has been quite successful in the prediction of field strength when the transmission path is obstructed by obstacles such as mountainous ridges [1–8].[2] In its usual form, however, this theory disregards the difference between vertical and horizontal polarization. Furthermore, the electrical properties of the diffracting obstacle are not considered since in effect, the obstacle is regarded as a "black screen" or absorbing knife edge. A brief mention of the various developments, both old and new, will be made in order to properly orient the reader.

Schelleng, Burrows, and Ferrell [1] in a now classic paper, applied knife edge Kirchhoff theory to the computation of the fields behind mountainous obstacles and other pronounced terrain features. The influence of the terrain in the immediate vicinity of the terminals was accounted for by the introduction of ground-reflected rays which are also diffracted by the obstacles.[3] A similar approach was made by Dickson, Egli, Herbstreit, and Wickizer [5], who demonstrated that the presence of an obstacle can, in some cases, produce an increase of field strength beyond that expected in the absence of the obstacle. This phenomenon has been described rather aptly as "obstacle gain" and has been used to advantage in the siting of the terminal and repeater stations in microwave relay links.

The Japanese workers [4,6] have also been very active in this field. Presumably, the mountainous features of their country have motivated much of this work. Matsuo [4] in particular, has applied the Kirchhoff theory to many geometrical forms including conical shaped obstacles. Some fundamental theoretical work has been carried out by Furutsu [9] who has presented solutions for diffraction by very general forms of obstacles.

S. O. Rice [11] has given a comprehensive solution for the diffraction of a plane wave by a perfectly conducting parabolic cylinder which was considered to be a more realistic model of a terrain obstacle. Particular attention was paid to the fields near the horizon plane on the boundary region between light and shadow. It was shown that to a first approximation, the diffraction pattern behind the obstacle was very similar to that for a knife edge. The main effect of the finite radius of curvature of the crest was to increase the field strength for vertical polarization and to decrease it for horizontal polarization. A similar observation had been made by Artmann [12] sometime earlier who employed a circular cylindrical model.

Still another approach to this problem was adopted by Norton, Rice, and Vogler [13]. They represented the diffracting obstacle first by a sphere for the case of a very large radius of curvature and then by a knife edge for vanishing small radii of curvature. A curve of diffraction loss as a function of radius of curvature was then drawn by interpolating between these two limiting cases. According to their results, the diminishing of the radii of curvature is ac-

[1] A preliminary version of this paper was presented at the International Conference on Wave Propagation, Liège, Belgium on October 8, 1958.

[2] Figures in brackets indicate the literature references at the end of this paper.

[3] A scheme which will suppress or modify these ground-reflected rays has been suggested by H. E. Bussey (Reflected Ray Suppressions, Proc. IRE **38**, 1453, 1950).

508098—59——5

companied by enormous increases in the field strength even though the separation between terminals and the angular distance is unchanged.

Refinements of Kirchhoff diffraction theory when applied to the diffraction by smooth cylindrical models were made by Neugebauer and Bachynski [14, 15]. The basic idea of their analysis is that the equivalent radiating aperture is illuminated not only by the incident rays, but from rays reflected from the illuminated side of the cylindrical crest. The subsequent radiation from this aperture plane, which extends from the apex of the crest upward to infinity, is again reflected from the shadow side of the crest. Neugebauer and Bachynski are quite willing to admit that this is not a rigorous procedure, but nevertheless, it leads to results which are in good agreement with experiment.

It is the purpose of the present paper to present a method for the computation of diffracted fields by convex surfaces which is both rigorous and easy to apply. The mathematical basis of this method was described in a previous paper [16]. This was an extension of the fundamental work of Van der Pol and Bremmer, and Fock. The reader is referred to the above quoted paper for an account of the early theoretical work.

Unfortunately, the existing solutions for the diffraction by spheres and cylinders are poorly convergent in the line-of-sight region. Consequently, these formal solutions require a great deal of numerical work despite the fact that they are mathematically elegant. A significant break-through was made when it was suggested that the complex-integral representation of the field was easier to evaluate by numerical means than attempting to sum the residues of the poles of the integrand. While this point was probably recognized by Van der Pol and Bremmer [17], in the 1930's, it was not until 1946 that Academician V. A. Fock actually demonstrated this in what is now regarded as a classic paper [18]. Fock's method was applied by the present authors to the computation of the radiation pattern of an antenna mounted on or near a convex lossy surface [16]. The present problem is really an extension of this work.

2. Formulation

The problem is to calculate the field at some point P exterior to the cylinder in terms of the field on its surface (see fig. 1a). Since the incident magnetic field $H^{\text{inc}}(\rho, \phi)$ is taken to have only a z component, the resultant field $H(\rho, \phi)$ also has only a z component. An immediate application of Green's theorem yields

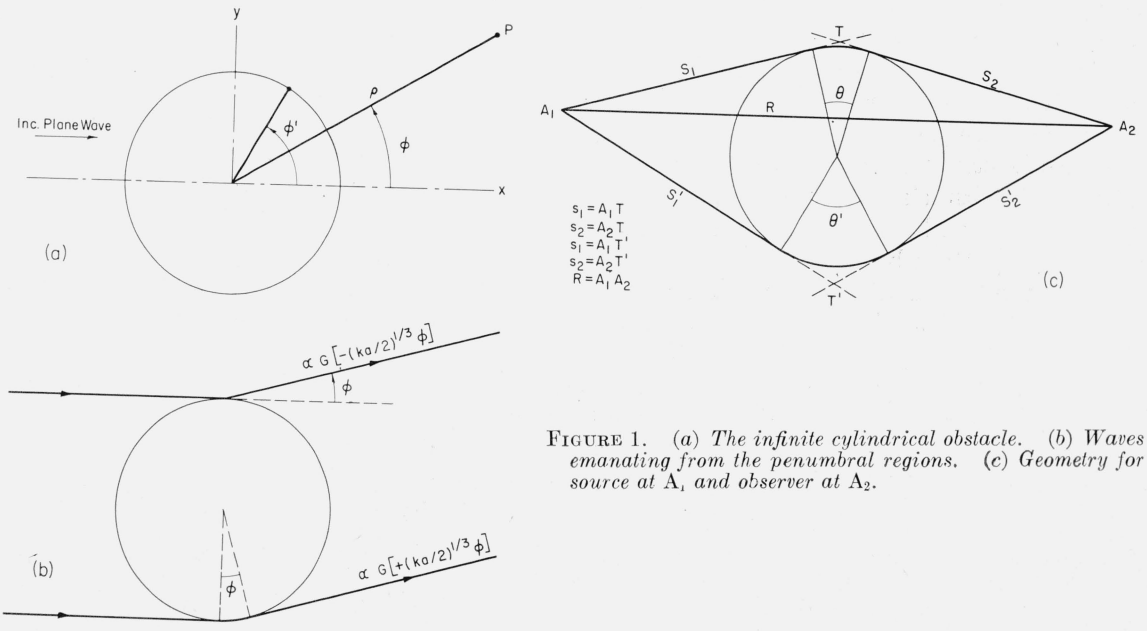

FIGURE 1. *(a) The infinite cylindrical obstacle. (b) Waves emanating from the penumbral regions. (c) Geometry for source at* A_1 *and observer at* A_2.

$$H_z(\rho,\phi)=H_z^{\text{inc}}(\rho,\phi)+a\int_0^{2\pi}\left[H_z(\rho',\phi')\frac{\partial}{\partial\rho'}Q(\rho,\phi;\rho',\phi')-Q(\rho,\phi;\rho',\phi')\left(\frac{\partial H_z(\rho',\phi')}{\partial\rho'}\right)\right]_{\rho'=a}d\phi', \tag{1}$$

where the Green's function is given by

$$Q(\rho,\phi;\rho',\phi')=-\frac{i}{4}H_0^{(2)}(k\hat{\rho}), \tag{2}$$

with

$$\hat{\rho}=[\rho^2+(\rho')^2-2\rho\rho'\cos(\phi-\phi')]^{1/2}.$$

The primed coordinates ρ', ϕ', with $\rho'=a$, refer to a variable point on the surface of the cylinder whereas ρ, ϕ, of course, refer to the position of the observer. The above integral formula can be simplified somewhat when the Leontovich boundary condition can be used [16]. Then

$$\frac{\partial H_z(\rho',\phi')}{\partial\rho'}\Big]_{\rho'=a}=i\epsilon_0\omega ZH_z(a,\phi), \tag{3}$$

where Z is the surface impedance of the cylinder and ϵ_0 is the permittivity of the surrounding space.[4] Invoking this approximation, the external field is expressed explicitly in terms of the surface field $H_z(a,\phi)$ which can be regarded as known. The evaluation of the integral, however, is not readily carried out unless certain restrictions are made. For the moment it will be assumed that the observer is at a large distance from the cylinder. Consequently,

$$\begin{aligned}Q&\cong-\frac{i}{4}\frac{1}{\sqrt{k\hat{\rho}}}e^{i[(\pi/4)-k\hat{\rho}]}\\&\cong\frac{e^{-i\pi/4}}{4\sqrt{k\rho}}e^{-ik\rho}e^{ik\rho'\cos(\phi-\phi')},\end{aligned} \tag{4}$$

where only the first term in the asymptotic expansion for $H_0^{(2)}(k\hat{\rho})$ has been retained.

In a previous paper [16], it was shown that

$$\begin{aligned}H_z(a,\phi')=H_0\sum_{m=0}^{\infty}e^{-ika\left[\left(\frac{\pi}{2}-\phi'\right)+2\pi m\right]}g\left[\frac{\pi}{2}-\phi'+2\pi m\left(\frac{ka}{2}\right)^{1/3}\right]\\+H_0\sum_{m=0}^{\infty}e^{-ika\left[\left(\phi'+\frac{\pi}{2}\right)+2\pi m\right]}g\left[\phi'+\frac{\pi}{2}+2\pi m\left(\frac{ka}{2}\right)^{1/3}\right],\end{aligned} \tag{5}$$

for the region $0\leqq|\phi'|\leqq(\pi/2)+\Delta\phi$, where $(\Delta\phi)^3<<1$. The function $g(X)$ occurring in the above expression is given by [16]

$$g(X)=\frac{1}{\sqrt{\pi}}\int_{\infty e^{-i2\pi/3}}^{\infty}\frac{e^{-iXt}}{w_1'(t)-qw_1(t)}dt, \tag{6}$$

where $w_1(t)$ and $w_1'(t)$ are Airy integrals defined in the appendix, and

$$q=-i\left(\frac{ka}{2}\right)^{1/3}Z/\eta_0,\quad\text{with }\eta_0\cong120\pi.$$

The quantity m can be physically regarded as the number of times a wave has crept around the cylinder. For $(ka)^{1/3}\pi>>1$, only the term $m=0$ need be retained. Furthermore, if $ka>>1$ and $|\phi|$ less and not near $\pi/2$ the geometrical optical approximation for $H_z(a,\phi')$ is applicable. This reads

$$H_z(a,\phi')\cong H_0(1+R_ve^{-ika\cos\phi'}), \tag{7}$$

---

[4] Equation (3) is strictly valid only when $(Z)<<120\pi$ but actually this is more stringent than necessary [16].

where R_v is a Fresnel reflection coefficient given by

$$R_v=-\frac{(Z/\eta_0)-\cos\phi'}{(Z/\eta_0)+\cos\phi'}. \tag{8}$$

3. Evaluation of the Field

The secondary or scattered field can thus be written in the following form

$$H_z^s(\rho,\phi)=\frac{e^{-i(k\rho-\pi/4)}}{2\sqrt{2\pi k\rho}}(\psi_1+\psi_2), \tag{9a}$$

where

$$\psi_1=\int_{-\pi}^{\infty}[\cos(\phi'-\phi)-kaZ/\eta_0]e^{-ika[(\pi/2)+\phi'-\cos(\phi'-\phi)]}g(X_1)d\phi' \tag{9b}$$

$$\psi_2=\int_{-\infty}^{\pi}[\cos(\phi'-\phi)-kaZ/\eta_0]\,e^{-ika[(\pi/2)-\phi'-\cos(\phi'-\phi)]}g(X_2)d\phi'. \tag{9c}$$

The phase in the integral ψ_1 has the form

$$\Omega(\phi')=ka[(\pi/2)+\phi'-\cos(\phi'-\phi)],$$

so that the stationary points are at $\phi'=\phi_n'=(4n-1)\ \pi/2+\phi$ for $n=0,\ 1,\ 2,\ 3\ \ldots$. The phase function is expanded about ϕ_n' and is of the form

$$\Omega(\phi')=ka[2\pi n+\phi+\tfrac{1}{6}(\phi'-\phi_n')^3],$$

neglecting terms containing higher power than the third. The integrals over ϕ' are now in the form of Airy integrals and thus ψ_1 and ψ_2 can be expressed in the form

$$\psi_1=\frac{-2\sqrt{\pi}\,e^{-i\pi/4}}{(ka/2)^{2/3}}\,e^{-ika\phi}\sum_{m=0}^{\infty}e^{-i2\pi mka}\,\hat{G}\left[\left(\frac{ka}{2}\right)^{1/3}\phi\right], \tag{10a}$$

$$\psi_2=\frac{-2\sqrt{\pi}\,e^{-i\pi/4}}{(ka/2)^{2/3}}\,e^{-ika\phi}\sum_{m=0}^{\infty}e^{-i2\pi mka}\,\hat{G}\left[-\left(\frac{ka}{2}\right)^{1/3}\phi\right], \tag{10b}$$

where

$$\hat{G}(X)=\frac{e^{-i\pi/4}}{\sqrt{\pi}}\int_{\infty\,e^{-i2\pi/3}}^{\infty}e^{-iXt}\frac{v'(t)-qv(t)}{w_1'(t)-qw_1(t)}\,dt, \tag{11}$$

where $w_1(t)$ and $v(t)$ are Airy integrals defined in the appendix. The quantity t is a new variable of integration.

The special cases corresponding to $q=0$ and $q=\infty$ lead directly to Goriainov [19] who assumed at the outset that the cylinder was perfectly conducting. These special cases are discussed in the subsequent text. The total field scattered by the cylinder is thus expressed by

$$H^s=-H_0\frac{e^{-ik\rho}}{\sqrt{k\rho}}(h_0+h_1), \tag{12}$$

where

$$h_0=\sqrt{\frac{2}{\pi}}\,e^{i\pi/4}\frac{\sin ka\phi}{\phi}, \tag{13}$$

and

$$h_1 = +\sqrt{2}\left(\frac{ka}{2}\right)^{1/3} \{e^{-ika\phi}G[(ka/2)^{1/3}\phi] + e^{ika\phi}G[-(ka/2)^{1/3}\phi] + e^{-ika(2\pi+\phi)}G[(ka/2)^{1/3}(2\pi+\phi)] + e^{-ika(2\pi-\phi)}G[(ka/2)^{1/3}(2\pi-\phi)] + \ldots]\}, \quad (14a)$$

where

$$G(X) = \hat{G}(X) + \frac{e^{-i\pi/4}}{2X\sqrt{\pi}}. \quad (14b)$$

The preceding results will now be generalized to include the case of a spherical wave incidence. The source is now imagined to be a magnetic dipole, located at $(\rho_0, \pi, 0)$, thus the radius of curvature of the incident wave at the origin is ρ_0. Equation (12) for the scattered field in the transverse plane $z=0$ is now simply generalized to spherical wave incidence by multiplying it by $\sqrt{\rho_0/(\rho+\rho_0)}$. This is valid for any form of cylindrical obstacle subject to ρ and ρ_0 both large compared to the maximum transverse dimension of the effective scattering region.[5] Thus

$$H_z^s \cong -H_0 \frac{e^{-ik\rho}}{(k\rho)^{1/2}}\left(\frac{\rho_0}{\rho_0+\rho}\right)^{1/2}(h_0+h_1), \quad (15)$$

where H_0 is the value of the incident field reckoned at the center of the cylinder and h_0 and h_1 are as defined above.

The portion of the scattered field proportional to h_0 corresponds to Kirchhoff diffraction since it can be readily predicted by physical optics. It is independent of the electrical properties of the obstacle (and thus independent of the surface impedance Z) and is proportional to the cross-sectional dimension of the obstacle for small deflection angles. The remaining part of the scattered field, proportional to h_1, can be regarded as a correction to Kirchhoff theory. When $ka \to \infty$, the ratio h_1/h_0 asymptotically approaches zero. For finite but large values of ka and small values of ϕ only the first two terms containing $G[(ka/2)^{1/3}\phi]$ and $G[-(ka/2)^{1/3}\phi]$ are significant. These can be interpreted as waves emanating from the penumbral regions on the cylinder as indicated in the sketch shown in figure 1b. In this case, the distances ρ and ρ_0 are both assumed very large compared to the transverse dimension of the obstacle (i.e., $2a$). To relax this condition, it is necessary to return to the original integral for the field and use the following far-field approximation for the Green's function:

$$Q \cong -\frac{i}{4}\frac{1}{\sqrt{k\hat{\rho}}}\, e^{i(\pi/4 - k\hat{\rho})}, \quad (16)$$

where $\hat{\rho}$ is not assumed to be large compared to $2a$ but is still large compared to the wavelength illustrated in figure 1c. Carrying through the analysis leads to

$$H_z = H_z^p + H_z^s \cong \frac{e^{-ikR}}{R}\,[F(X,u) + F(X',u')], \quad (17)$$

with

$$F(X,u) = \frac{e^{i\pi/4}}{\sqrt{\pi}}\int_\alpha^\infty e^{-i\alpha^2}d\alpha - \frac{G(X)}{u}\, e^{-iu^2}, \quad (18)$$

where

$$u = \frac{\alpha}{X} = \left(\frac{2ks_1s_2}{s_1+s_2}\right)^{1/2}\frac{(2/ka)^{1/3}}{2},$$

and

$$X = (ka/2)^{1/3}\theta.$$

Equation (18) is only valid when u is somewhat greater than unity. A more accurate form is obtained when $G(X)$ is replaced by $G(X) - \frac{i}{4u^2}\frac{\partial^2 G(X)}{\partial^2 X}$.

[5] See J. R. Wait, Appl. Sci. Research **B.4,** 464 (1955) for example.

The function $F(X', u')$ is the same form as $F(X, u)$, and u' and X' are defined by

$$u'=\frac{\alpha'}{X'}=\left(\frac{2ks_1's_2'}{s_1'+s_2'}\right)^{1/2}\frac{(2/ka)^{1/3}}{2},$$

and

$$X'=(ka/2)^{1/3}\theta'.$$

The quantities s_1 and s_2 are the linear distances from the source A_1 and the receiver A_2 measured to the intersection of tangent planes of the surface of the cylinder as sketched in figure 1c. Similar remarks apply to the primed quantities.[6] The quantity R is the linear distance separating A_1 and A_2.

It should be noted that when A_1 and A_2 recede to infinity, the earlier (Fraunhofer) solution is retrieved as a special case. To effect this transition, it is convenient to use the asymptotic relation

$$[uF(X, u)]\cong e^{-i\alpha^2}\left[\frac{e^{-i\pi/4}}{2\sqrt{\pi X}}-G(X)\right] \quad \text{for large positive } \alpha \text{ and} \tag{19}$$

$$\cong e^{-i\alpha^2}\left[u+\frac{e^{-i\pi/4}}{2\sqrt{\pi X}}-G(X)\right] \quad \text{for large negative } \alpha.$$

Up to this point the analysis has been developed explicitly for the incident magnetic field vector directed along the axis of the cylinder. The results can be transformed to the case for the incident electric field vector directed along the axis of the cylinder by making the following transformation

$$H_z^{\text{inc}}(\rho, \phi)\rightarrow E_z^{\text{inc}}(\rho, \phi)$$

$$H_z^s\ (\rho, \phi)\rightarrow E_z^s\ (\rho, \phi)$$

$$\left[q=-i\left(\frac{ka}{2}\right)^{1/3}\left(\frac{Z}{\eta_0}\right)\right]\rightarrow\left[q=-i\left(\frac{ka}{2}\right)^{1/3}\left(\frac{\eta_0}{Z}\right)\right].$$

For metallic surfaces, $q\cong 0$ for H parallel polarization and $q\cong\infty$ for E parallel polarization, and these limiting cases are referred to in the following section as vertical and horizontal polarizations, respectively.

4. Numerical Results

Basic to the present work is the function $G\ (X)$. In the region near $X=0$, the relevant integrals cannot apparently be evaluated in closed form. The integrands are quite well behaved however, and it is not too difficult to evaluate them by numerical means. In figures 2a and 2b the real and imaginary parts of $G\ (X)$ are plotted as a function of X for $q=0$ and $q=\infty$, respectively.

Before discussing the diffraction pattern, it is of interest to consider the behavior of the field along the horizon plane. Clearly, this corresponds to $\theta=0$, $X=0$, and $\alpha=0$. The function $F\ (\alpha)$ then becomes

$$F(0)=\frac{1}{2}-\frac{G(0)}{u}, \tag{20}$$

where

$$u=\left(\frac{2ks_1s_2}{s_1+s_2}\right)^{\frac{1}{2}}\frac{(2/ka)^{\frac{1}{3}}}{2}, \text{ as before.}$$

Numerical integration yields the following values: for $q=0$, $G\ (0)=-0.295+i\ 0.0811$; and

[6] θ and θ' are the angles subtended by the tangent planes as indicated in figure 1c. They are referred to sometimes as angular distances and expressed in milliradians.

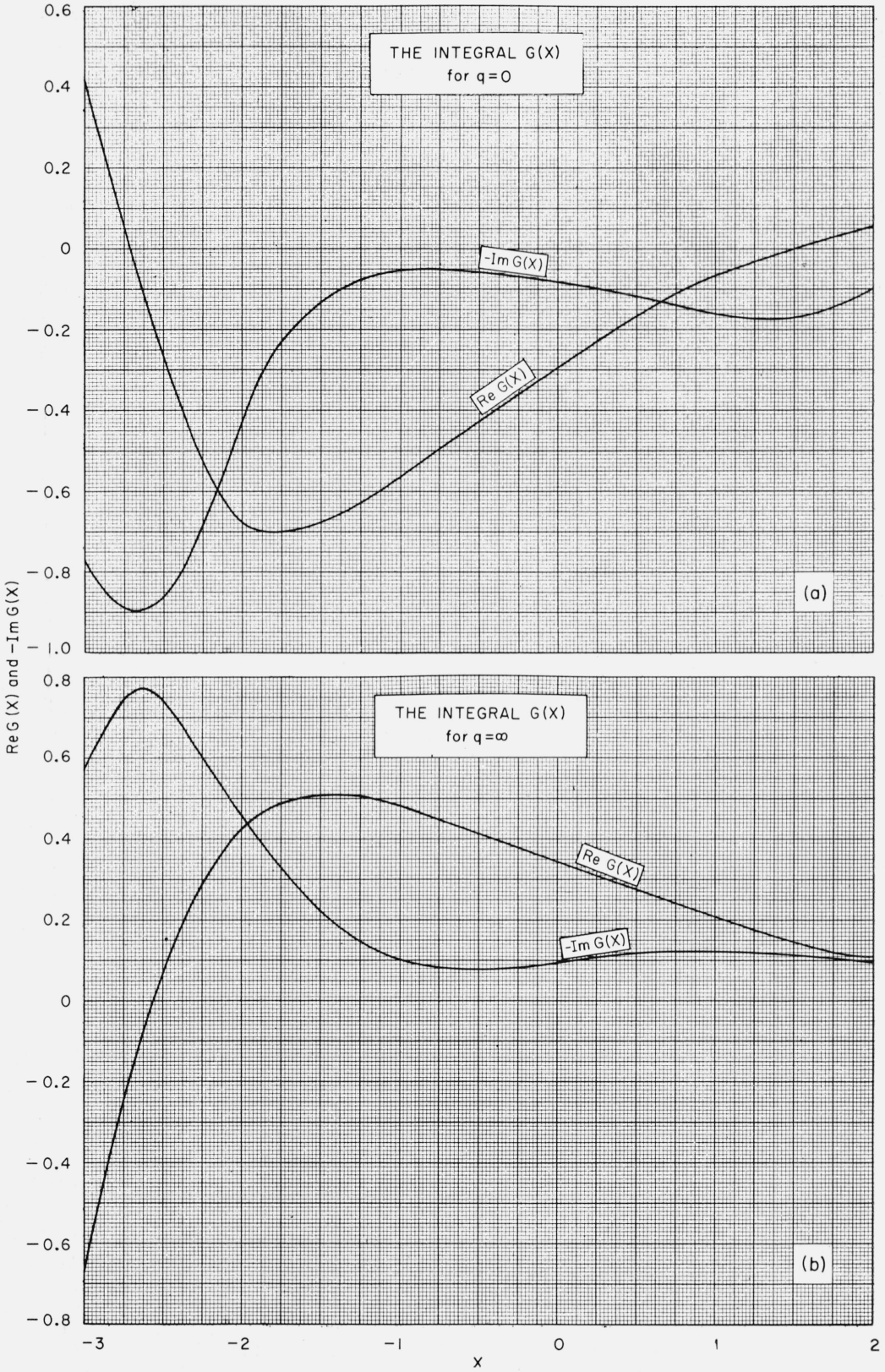

FIGURE 2. (*a*) *Real and imaginary parts of the integral* G(X) *as a function of* X *for* q = 0. (*b*) *Real and imaginary parts of the integral* G(X) *as a function of* X *for* q = ∞.

for $q=\infty$, $G(0)=0.344-i\,0.0918$. This indicates that for vertical polarization (corresponding to $q=0$) with a metallic convex surface, the field along the shadow boundary is increased above that for a knife edge. The converse is true for horizontal polarization (corresponding to $q=\infty$). The increase or reduction from ½ is approximately the real part of the function $[-G(0)/u]$. Therefore for $q=0$, $|F(0)|\cong 0.500+(0.295/u)$ and for $q=\infty$, $|F(0)|\cong 0.500-(0.344/u)$. It is of interest to compare this departure from ½ with Rice's prediction using a parabolic cylinder model. The agreement is good if we equate the curvature of the apex of his parabolic cylinder with our a. It is also noted that his assumed plane-wave incidence is equivalent to moving our source to infinity (i.e., $d_1=\infty$). Then on identifying Rice's h with $ka/2$ and his Λ with $[(s_1+s_2)/(2\pi k s_1 s_2)]^{\frac{1}{2}}$, we find according to Rice for $q=0$, $|F(0)|\cong 0.500+(0.296/u)$ and for $q=\infty$, $|F(0)|\cong 0.500-(0.342/u)$, being in close agreement with our values quoted above. On the other hand, Artmann, using a circular cylindrical model, gives for $q=0$, $|F(0)|\cong 0.500+(0.165/u)$ and for $q=\infty$, $|F(0)|\cong 0.500-(0.33/u)$. The disagreement in the case for $q=0$ with our result should be noted. It is suggested that the asymptotic approximation for the Hankel functions used by Artmann is not fully justified.

Neugebauer and Bachyinski have also computed a value on the shadow boundary using a semiempirical modification to Kirchhoff theory. Again transferring to our notation they would give[7]

$$\text{for } q=0, \qquad |F(0)|\cong 0.500+\frac{0.271}{u}, \quad \text{and}$$

$$\text{for } q=\infty, \qquad |F(0)|\cong 0.500-\frac{0.282}{u}.$$

The agreement of these values with ours (and those of Rice) is reasonable in view of the entirely different theoretical approaches employed. It is probable that at least part of the discrepancies can be attributed to the nonvalidity of some of the geometrical-optical arguments used by Neugebauer and Bachynski.

5. Diffraction Patterns

The diffraction pattern behind the obstacle is specified by the behavior of the function $F(X, u)$ as α or uX varies. The amplitude $|F(X, u)|$ itself and the resulting diffraction loss L_d are plotted in figure 3a for various values of u with $q=0$ and ∞. As u tends to infinity, the patterns approach the Kirchoff form described by the function $F_0(\alpha)$. Since the function $F_0(\alpha)$ occurs frequently in what follows, its real and imaginary parts are plotted in figure 3b.

The diffraction pattern behind a metallic cylindrical model of a mountain crest has been measured by Neugebauer and Bachynski in the K-band frequency range. For purposes of comparison, they also duplicated the experiment using a thin metallic sheet which was essentially equivalent to a knife edge. Their results for $ka=239$ are shown in figure 4a and 4b for vertical polarization ($q=0$) and horizontal polarization ($q=\infty$), respectively. The ordinates are relative power and the abscissa are distance d_2 measured from the crest to the observer. The quantity h is the vertical displacement of the receiver above or below the horizon plane. In both figures 4a and 4b the source which is a transmitting horn is at a fixed location, being a distance d_1 ($=150\lambda$) from the crest. Values calculated from eq (18) are also shown on the curves. The agreement is reasonably good.

Neugebauer and Bachynski also measured the fields behind the crest for various values of the curvature parameter ka. This is shown in figure 5 where the ordinate is relative power and the abscissa is the deflection angle θ. The corresponding calculated curves are also shown in figure 5, taking $d_1=150\lambda$ and $d_2=113\lambda$. The agreement is still fairly good and probably is within experimental error. These curves illustrate in a striking way the influence of curvature on the diffraction fields. In the case of horizontal polarization and deep in the shadow, the

[7] Their quantity 'A'$=-8\pi^{1/2}\,2^{-1/3}$ times the real part of our $G(0)$.

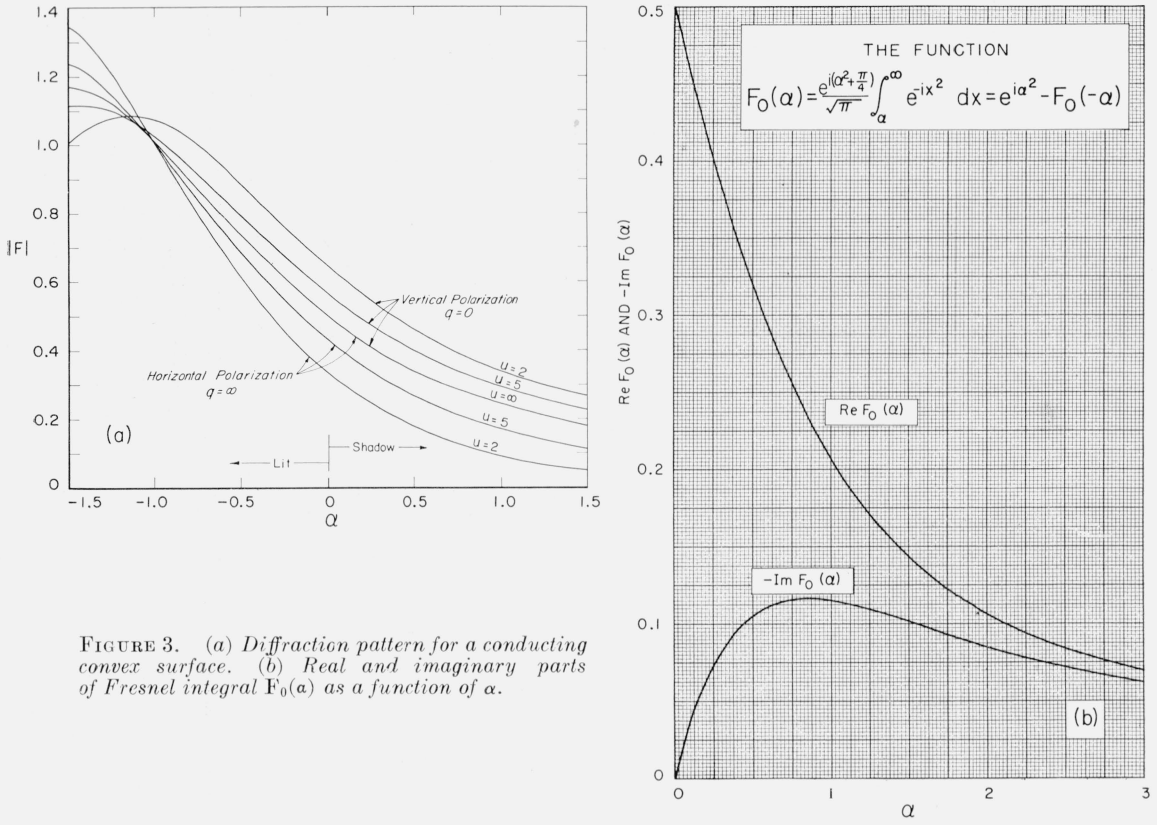

FIGURE 3. *(a) Diffraction pattern for a conducting convex surface. (b) Real and imaginary parts of Fresnel integral* $F_0(\alpha)$ *as a function of* α.

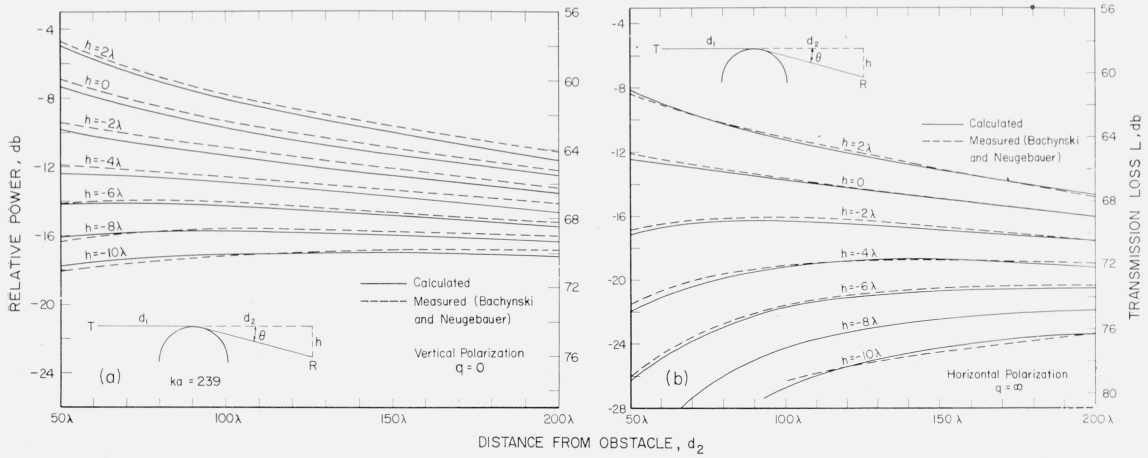

FIGURE 4. *(a) Power distribution behind a cylindrical obstacle. (b) Power distribution behind a cylindrical obstacle.*

finite radius of curvature greatly reduces the fields below the Kirchhoff or knife-edge value. This is in accord with the results of Norton, Rice, and Vogler [13].

6. Further Numerical Results

To obtain results for finite conductivity, it is necessary to evaluate the relevant integrals for finite values of q. For the case of H-parallel or vertical polarization

$$q=-i\left(\frac{ka}{2}\right)^{1/3} Z/\eta_0,$$

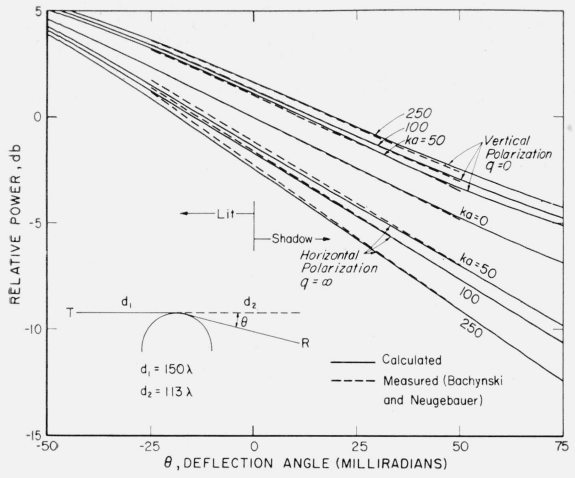

FIGURE 5. *Effect of curvature on diffraction by a convex surface.*

where Z is the surface impedance. Now if the surface is a good conductor

$$Z \cong (i\mu\omega/\sigma)^{1/2},$$

subject to $\sigma >> \epsilon\omega$. That is, displacement currents in the conductor are neglected. The consequence of this approximation was discussed in some detail in a previous paper devoted to this subject [16]. Following the earlier notation

$$q \cong |q| e^{-i\pi/4} = 2^{1/6} A e^{-i\pi/4},$$

where

$$A = (ka)^{1/3} \left(\frac{\epsilon_0 \omega}{2\sigma}\right)^{1/2},$$

is the "loss factor" for the surface. It is seen that for infinite conductivity, A is zero. On the other hand, for very poor conductivity and large values of ka, the "loss factor", A, may approach infinity. These two limiting cases correspond to $q=0$ and $q=\infty$, respectively, and were discussed in the previous section. More usually A takes some intermediate value.

For the general case

$$\hat{G}(X) = \hat{G}_1(X) + \hat{G}_2(X) \tag{21}$$

$$G(X) = \hat{G}_1(X) + \hat{G}_3(X), \tag{22}$$

where

$$\hat{G}_1(X) = \frac{e^{-i\pi/4}}{\sqrt{\pi}} \int_0^\infty e^{-iXt} \frac{v'(t) - qv(t)}{w_1'(t) - qw_1(t)} dt, \tag{23}$$

$$\hat{G}_2(X) = \frac{e^{i3\pi/4}}{2X\sqrt{\pi}} + \hat{G}_3(X), \tag{24}$$

$$\hat{G}_3(X) = \frac{e^{i\pi/12}}{\sqrt{\pi}} \int_0^\infty e^{(-Xt/2)(\sqrt{3}-i)} \left[\frac{v'(t) - qe^{-2\pi i/3} v(t)}{w_2'(t) - qe^{-2\pi i/3} w_2(t)}\right] dt. \tag{25}$$

The above relations follow immediately from eq (11) and (14b). The real and imaginary parts of the integrals $\hat{G}_1(X)$ and $\hat{G}_3(X)$ were evaluated numerically using tabulated values of the Airy integral functions. For the present purpose only the real and imaginary parts of the function $G(X)$ are required.

As mentioned above, the field along the horizon plane is of special interest. Expressed as a ratio to the free-space field, this can be written

$$F(0)=\frac{1}{2}-\frac{G(0)}{u}.$$

The real and imaginary parts of G (0) are plotted in figure 6 in the form of an Argand diagram. Various values of A are shown on the curve. The left-hand portion of the curve (i.e., smaller A values) corresponds to an increase over the knife edge value. On the other hand the right-hand portion (i.e., larger A) corresponds to a decrease below the knife-edge field. It is of interest to note that for an A value of about 0.4 the magnitude of the diffraction field is almost the same as that of the knife-edge field. Associated with these intermediate values of A, however, are appreciable phase shifts which correspond to a lag relative to the phase of the knife-edge field. The end points of the curve corresponding to $q=0$ and $q=\infty$ were discussed in the earlier section.

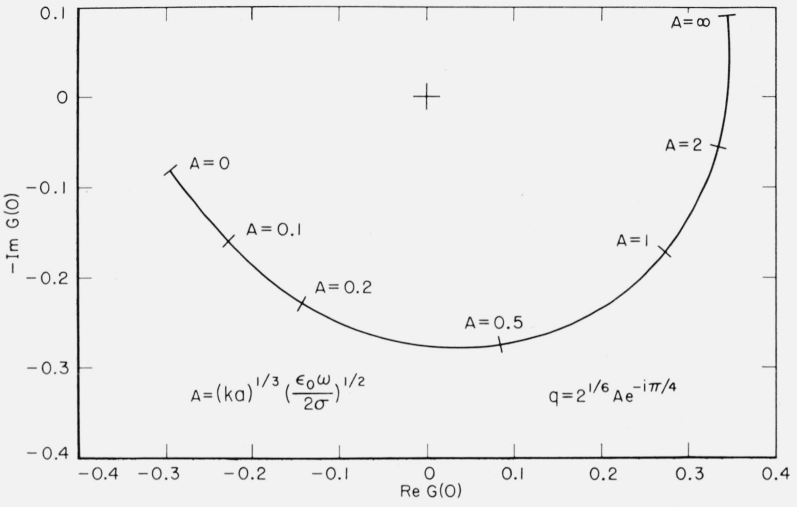

FIGURE 6. *Integral* G(O) *plotted in the complex plane for various values of the conductivity parameter* A.

Applicable to vertical polarization.

The real and imaginary parts of G (X) are shown plotted in figures 7a and 7b, respectively, as a function of X for various values of A.

The diffraction pattern defined by $|F(X, u)|$ can thus be readily computed for any value of A. Examples of these are shown in figures 8a, 8b, and 8c for u equal to 2, 5, and 10, respectively.

The preceding results indicate that the influence of finite conductivity can be marked for H-parallel or vertical polarization. For purposes of illustration, the displacement currents were neglected so that q has a phase angle of -45 deg. For poorer conductivities this restriction may be violated and the numerical results are not strictly applicable although they can be used for approximate estimates as long as the conduction currents are at least greater than the displacement currents. (i.e., $\sigma > \epsilon\,\omega$). In this case, the equation for A should be replaced by

$$A=(ka)^{1/3}\left(\frac{\epsilon_0\omega}{\sqrt{\sigma^2+\epsilon^2\omega^2}}\right)^{1/2}\frac{1}{2^{1/2}}.$$

The influence of finite conductivity for E-parallel or horizontal polarization is negligible for most cases since $|q|$ is always very large compared to unity.

7. Concluding Remarks

A theory for diffraction of electromagnetic waves by a smooth and convex lossy obstacle has been presented. The model employed for computation is a circular cylinder of finite conductivity.

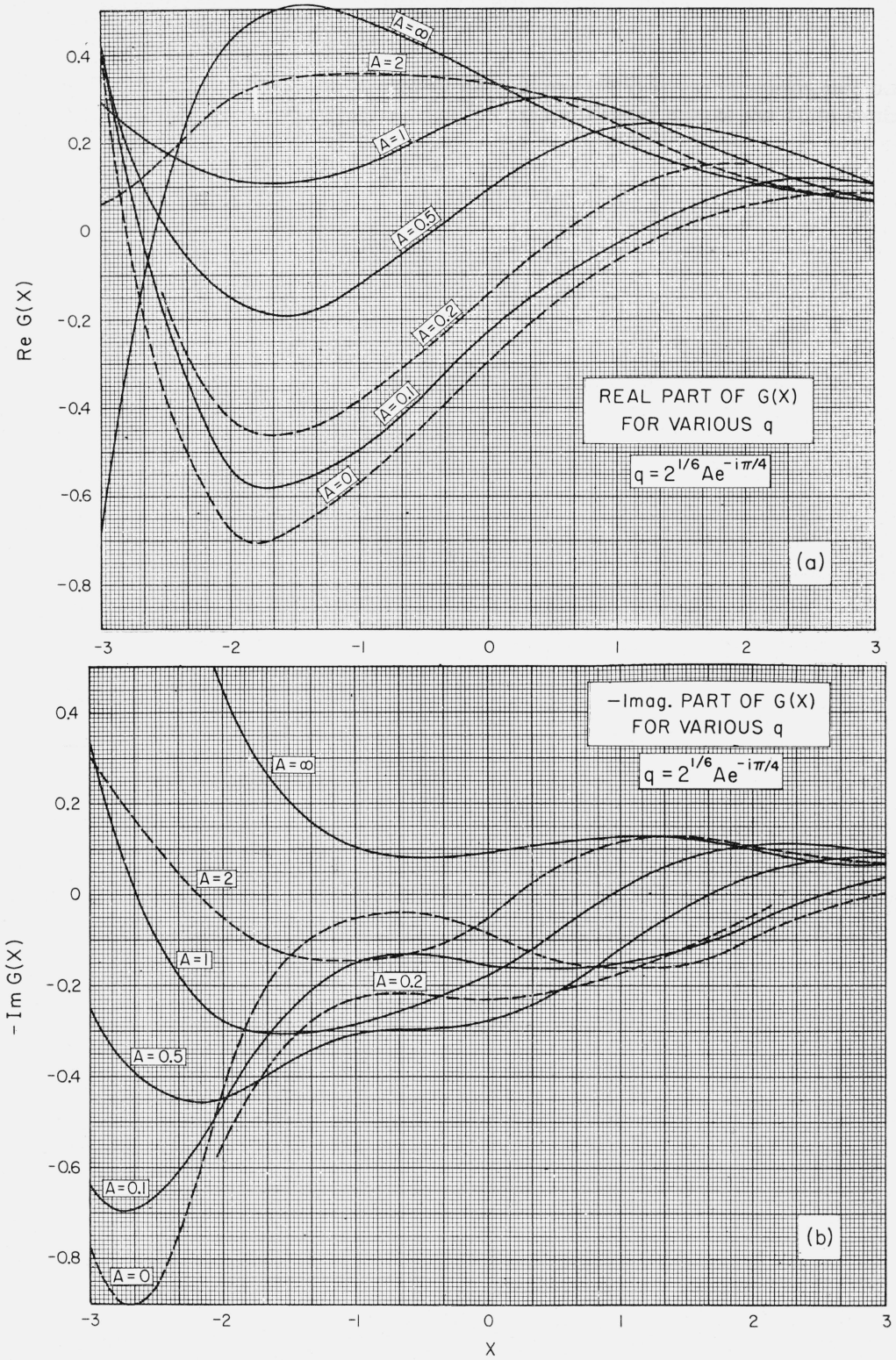

FIGURE 7. *(a) The real part of the function* G(X) *as a function of* X *for various values of the conductivity parameter A. (b) The imaginary part of the function* G(X) *as a function of* X *for various values of the conductivity parameter A.*

Both (a) and (b), applicable to vertical polarization.

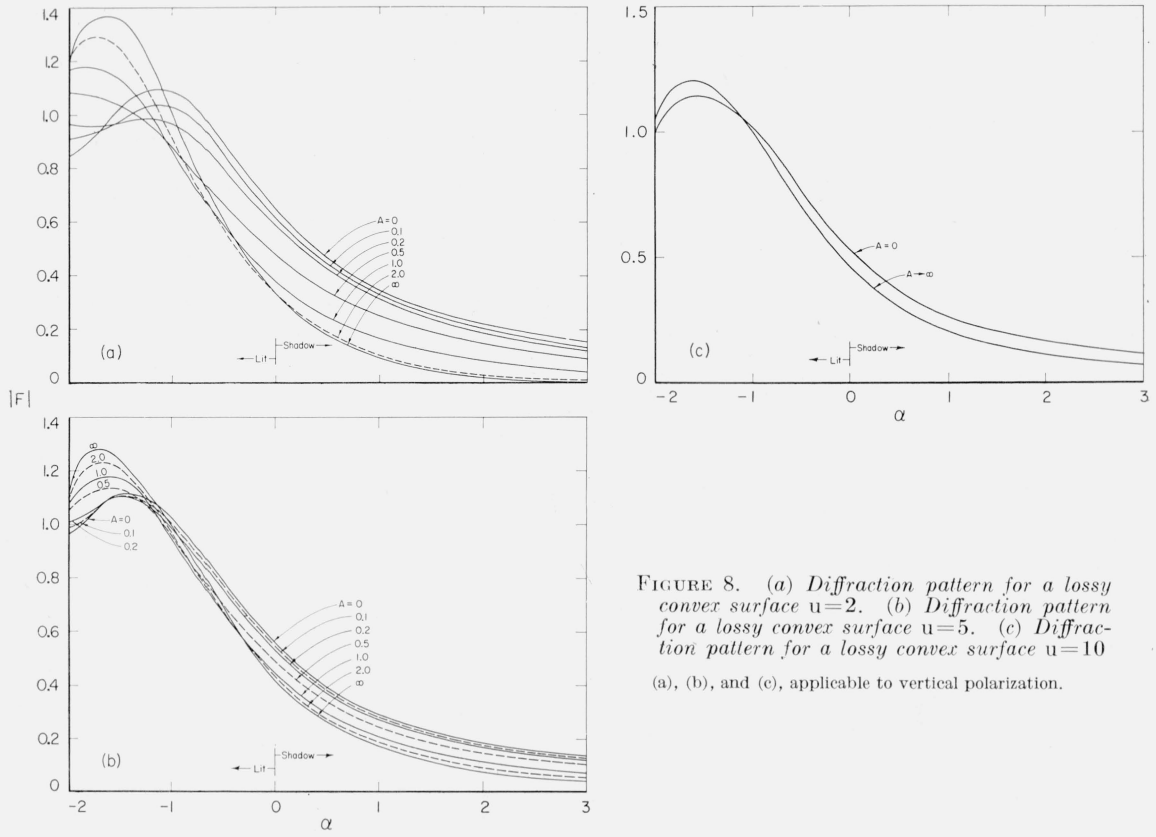

FIGURE 8. *(a) Diffraction pattern for a lossy convex surface* u=2. *(b) Diffraction pattern for a lossy convex surface* u=5. *(c) Diffraction pattern for a lossy convex surface* u=10

(a), (b), and (c), applicable to vertical polarization.

Probably the most important conclusion is that the influence of finite curvature of the diffracting metallic obstacle is to add a positive correction to the Kirchhoff computed field for a vertically polarized incident field, whereas the correction is negative for horizontally polarized incident field. The increase or decrease of amplitude from the Kirchhoff result is accompanied by a corresponding change of phase which may be important in certain applications.

The influence of finite conductivity is appreciable for vertical polarization and the curves presented in the paper may be used to compute this effect. In general, the ohmic loss tends to reduce the resultant diffracted field. In the case of a horizontal polarization, the finite conductivity has a negligible effect and the curves presented in the present paper for $q=\infty$ may be used directly.

While the present results are formally restricted to a diffracting surface of constant curvature, it can be expected that the results can be used for generally convex surfaces if the curvature is slowly changing. For example, it may be noted that the diffraction pattern has the same approximate analytical form for a circular cylinder, a sphere and a parabolic cylinder. At least this is true if the radius of curvature is large compared to the wavelength and the deflection angles are small. Deep in the shadow zone, this similarity principle breaks down and the field depends on the rate of change of the curvature. This aspect of the problem has been discussed recently by Wu [24] who has generalized some of the quasi-geometrical concepts of Keller [25]. As Wu points out, however, for small deflection angles (i.e., reasonably near line-of-sight) the diffraction field is not critically dependent on the analytical form of the surface provided it is sufficiently smooth. It can be expected that this will also be true for lossy obstacles.

8. Appendixes

8.1. Definition of Airy Integrals

The Airy integrals used in the above analysis can be represented by the following contour integrals

$$w_1(t)=\frac{1}{\sqrt{\pi}}\int_{\infty e^{i2\pi/3}}^{\infty} e^{\alpha}ds=u(t)-iv(t) \tag{26}$$

$$w_1'(t)=\frac{1}{\sqrt{\pi}}\int_{\infty e^{i2\pi/3}}^{\infty} se^{\alpha}ds=u_1'(t)-iv'(t) \tag{27}$$

$$w_2(t)=\frac{1}{\sqrt{\pi}}\int_{\infty e^{-i2\pi/3}}^{\infty} e^{\alpha}ds=u(t)+iv(t) \tag{28}$$

$$w_2'(t)=\frac{1}{\sqrt{\pi}}\int_{\infty e^{-i2\pi/3}}^{\infty} se^{\alpha}ds=u'(t)+iv'(t) \tag{29}$$

where $\alpha=st-s^3/3$.

The functions $u(t)$, $v(t)$, $u'(t)$, and $v'(t)$ have been tabulated by Fock [20] for real values of t.

8.2. Comparison With Results for a Spherical Model

The previous discussion has been based on a cylindrical model. It is of interest to compare these results with those of Fock [21] who employed a spherical model. To facilitate this discussion, it is desirable to review briefly Fock's work as it pertains to this particular problem. The notation will be changed to be consistent with the rest of the present paper.

The source is represented as a vertical electric dipole located at $r=a+h_1$ with respect to a sphere at $r=a$. (r, $\bar{\theta}$, ϕ are the usual spherical coordinates with origin at the center of the sphere and the axis in the direction of the dipole.) The great circle distance between the source and the receiver is denoted by s which, of course, is equal to $a\theta$. The receiver is located at $r=a+h_2$. In Fock's theory the following parameter is consistently employed

$$M=(ka/2)^{1/3},\quad x=M(s/a)=M\bar{\theta},$$

$$y_1=kh_1/M \text{ and } y_2=kh_2/M.$$

The fields for this geometry can be derived from a single scalar function U which has the following form

$$U=e^{-ikR}/R+U^s,$$

where R is the distance from the source to the observer. The first term is a spherical wave and represents the primary influence whereas the quantity U^s is the secondary influence resulting from the presence of the spherical body. The rigorous analytical expression for U^s is well known, being given first by G. N. Watson in a form of a very slowly converging series. The transformation of this series into a complex integral had also been accomplished by Watson who suggested that a new series could be evolved if the contour was deformed round a set of complex poles. This results in the now well-known residue series which has been studied extensively. Rather than deforming the contour Fock decided that the complex integral could be employed directly. He approximated the spherical Bessel functions by an Airy integral approximation. This is equivalent to Van der Pol's and Bremmer's "Hankel approximation" which involved Hankel functions of order one-third. This representation is valid when the argument and the order of the spherical Bessel functions are very large, but nearly the same magnitude. This means that the heights h_1 and h_2 are small compared to the radius

a which itself must be very large compared to the wavelength. Fock is then able to write U in the following form

$$U=\frac{e^{-iks}}{\sqrt{sa\sin\bar{\theta}}}V$$

where V is an attenuation function which is expressed conveniently as the sum of two parts, such that $V=V_1+V_2$, where V_1 does not depend on the electrical properties of the sphere and V_2 is dependent on these properties. The explicit representation for these integrals are

$$V_1=\left(\frac{ix}{\pi}\right)^{1/2}\left[\frac{1}{2i}\int_{C_1}e^{-ixt}w_1(t-y_2)w_2(t-y_1)dt+\int_{C_2}e^{-ixt}w_1(t-y_2)v(t-y_1)dt\right], \tag{30}$$

and

$$V_2=-\left(\frac{ix}{\pi}\right)^{1/2}\left[\frac{1}{2i}\int_{C_1}e^{-ixt}\frac{w_2'(t)-qw_2(t)}{w_1'(t)-qw_1(t)}w_1(t-y_1)w_1(t-y_2)dt\right.$$

$$\left.+\int_{C_2}e^{-ixt}\frac{v'(t)-qv(t)}{w_1'(t)-qw_1(t)}w_1(t-y_1)w_1(t-y_2)dt\right], \tag{31}$$

where $w_1(t)$, $w_2(t)$, and $v(t)$ are Airy integrals defined in appendix 8.1 and q is as defined previously. The contour C_1 is the straight line segment in the t plane from $\infty\exp(-i2\pi/3)$ to 0, and C_2 is the segment along the real axis from 0 to ∞. By some ingenious manipulations, the above integral representation V_1 is shown by Fock to correspond to Kirchhoff diffraction and consequently, V_2 can be regarded as the correction to the Kirchhoff theory. More explicitly

$$V_1\cong\frac{\sqrt{x}}{(y_1y_2)^{1/4}}e^{-i\omega_0}uF_0(\alpha)\text{ for }\alpha>0 \tag{32}$$

and

$$V_1\cong e^{-i\omega_0}\left[e^{i\alpha^2}-\frac{\sqrt{x}}{(y_1y_2)^{1/4}}uF_0(-\alpha)\right]\qquad\text{for }\alpha<0 \tag{33}$$

where $\omega_0\cong k(R-s)$, $u=(y_1y_2)^{1/4}/(\sqrt{y_1}+\sqrt{y_2})^{1/2}$ and $\alpha=u(x-\sqrt{y_1}-\sqrt{y_2})$. The function involves the Fresnel integral which is defined by

$$F_0(\alpha)=\frac{ei^{\left(\alpha^2+\frac{\pi}{4}\right)}}{\sqrt{\pi}}\int_\alpha^\infty e^{-ix^2}dx. \tag{34}$$

It is now possible to express V_2 in terms of the integral $G(X)$ encountered in the previous section. In fact,

$$V_2\cong-\frac{\sqrt{x}}{(y_1y_2)^{1/4}}e^{-i\omega_0}G(X), \tag{35}$$

where $X=\alpha/u=x-\sqrt{y_1}-\sqrt{y_2}$. Equations (33) and (35) given above for V_1 and V_2, respectively, are valid if x, y_1, and y_2 are all large compared to unity, but in such a way that X or $x-\sqrt{y_1}-\sqrt{y_2}$ is finite. It is also important to remember that these particular results are only valid for h_1 and h_2 small compared to a. This fact appears to have been overlooked in a recent paper by Kalinin [22]. In many physical situations one is interested in computing diffraction by a spherical surface when h_1 and h_2 are comparable or even large compared to a. It is quite easy, however, to relax this restriction if the proper asymptotic form of the spherical Hankel functions $h_{\nu-1/2}(\rho)$ is employed and ρ is either $a+h_1$, or $a+h_2$ in Fock's work. First it should be noted that

$$h_{\nu-1/2}(\rho)=\sqrt{\frac{\pi kb}{2}}H_\nu^{(2)}(\rho), \tag{36}$$

where $H_\nu^{(2)}(\rho)$ is the Hankel function of the second kind of order ν and argument ρ. The Debye second order representation for the Hankel function $H_\nu^{(2)}(kb)$ is now employed and leads to the approximation

$$h_{\nu-1/2}(\rho) \cong \frac{e^{-i(\xi-\pi/4)}}{(1-\nu^2/\rho^2)^{1/4}}, \tag{37}$$

where $\xi=(\rho^2-\nu^2)^{1/2}-\nu \cos^{-1}(\nu/\rho)$, being valid when $(\rho^2-\nu^2)>>\rho^{3/2}$. With this change, it is now possible to write the solution in the form

$$U=\frac{e^{-ikR}}{R} F, \tag{38}$$

where

$$F \cong [F_0(\alpha)+F_1]e^{-i\alpha^2}, \tag{39}$$

$$F_1=-G(X)/u, \tag{40}$$

$$u=\frac{a}{X}=\left(\frac{2ks_1s_2}{s_1+s_2}\right)^{1/2} \frac{(2/ka)^{1/3}}{2}, \tag{41}$$

and

$$X=(ka/2)^{1/3}\theta. \tag{42}$$

θ is the angular distance as usually defined, [8] and s_1 and s_2 are the linear distances measured from the source and the observer to the intersection of their tangent planes as in the previous section.

The research reported herein was sponsored in part by the U.S. Air Force Cambridge Research Center, Air Research and Development Command.

9. References

[1] J. C. Schelleng, C. R. Burrows and E. B. Ferrell, Ultra shortwave propagation, Proc. IRE **21,** 427 (March 1933).

[2] H. Selvidge, Diffraction measurements at ultra-high frequencies, Proc. IRE **29,** 10 (January 1941).

[3] K. A. Norton, M. Schulkin, and R. S. Kirby, Ground wave propagation over irregular terrain at frequencies above 50 Mc, Reference C to the report of the Ad Hoc Committee of the Federal Communications Commission for the evaluation of the radio propagation factors concerning the television and frequency modulation broadcasting services in the frequency range between 50 and 250 Mc (June 6, 1949).

[4] S. Matsuo, The method of calculating vhf field intensity and research on its variations, Report of the Electrical Communications Laboratory 621.30.001.6(047.3), Ministry of Telecommunications, Tokyo, Japan, (August 1950).

[5] F. H. Dickson, J. J. Egli, J. W. Herbstreit, and G. S. Wickizer, Large reductions of vhf transmission loss and fading by the presence of a mountain obstacle in beyond line-of-sight paths, Proc. IRE **41,** 967, (1953). See comments on this paper by J. H. Crysdale Proc. IRE **43,** 627 (1955).

[6] T. Kono, Y. Uesugi, M. Hirai, S. Niwa, and H. Irie, Measurement of field intensity of vhf radio waves behind Mt. Fugi, J. Radio Research Labs. (Tokyo) **1,** 1 (1954), Ministry of Postal Services, Tokyo, Japan.

[7] K. Bullington, Radio propagation at frequencies above 30 megacycles, Proc. IRE **35,** 1122 (1947).

[8] R. S. Kirby, H. T. Dougherty, and P. L. McQuate, Obstacle gain measurements over Pike's Peak at 60 to 1,046 Mc, Proc. IRE **43,** 1467 (1955).

[9] K. Furutsu, On the multiple diffraction by spherical mountains, J. Radio Research Labs. (Tokyo) **3,** 331 (1956).

[10] J. H. Crysdale, J. W. B. Day, W. S. Cook, M. E. Psutka, and P. E. Robillard, An experimental investigation of the diffraction of electromagnetic waves by a dominating ridge, IRE Trans. **AP–5,** 203 (1957).

[11] S. O. Rice, Diffraction of plane radio waves by a parabolic cylinder, Bell System Tech. J. **33,** 417 (1954).

[12] K. Artmann, Beugung polarisierten lichtes an blender endlicher dicke in gebiet der schattengrenze, Z. Physik **127,** 468 (1950).

---

[8] See figure 1c, for example. θ should not be confused with the spherical angle coordinate $\bar{v}$.

[13] K. A. Norton, P. L. Rice, and L. E. Vogler, The use of angular distance in estimating transmission loss and fading range for propagation through a turbulent atmosphere over irregular terrain, Proc. IRE **43,** 1480 (1955).

[14] H. E. J. Neugebauer and M. P. Bachynski, Diffraction by smooth cylindrical mountains, Proc. IRE **46,** 1619 (1958).

[15] I. P. Shkarofsky, H. E. J. Neugebauer, and M. P. Bachynski, IRE Trans. **AP–6,** 341 (1958).

[16] J. R. Wait and A. M. Conda, Pattern of an antenna on curved lossy surface, IRE Trans. **AP–6,** 348 (1958).

[17] H. Bremmer, Terrestrial radio waves, (Elsevier Publishing Co., Amsterdam, 1949). A comprehensive review of the early work of Watson, Van der Pol, and Bremmer is given.

[18] V. A. Fock, The field of a plane wave near the surface of a conducting body, J. Phys. U.S.S.R. **10,** 399 (1946).

[19] A. S. Goriainov, Diffraction of plane electromagnetic waves on a conducting cylinder, Radiotekh. i Elektron. **3,** 603 (1958). The paper, restricted to plane-wave incidence and perfect conductivity, is a limiting case of the present analysis.

[20] V. A. Fock, Diffraction of radio waves around the earth's surface (Academy of Sciences, U.S.S.R., 1946).

[21] V. A. Fock, Fresnel diffraction from convex bodies, Uspekhi Fiz. Nauk **43,** 587 (1951). A sphere model is used in a study restricted to antenna heights small compared to the radius of curvature.

[22] A. I. Kalinin, Approximate methods of computing field strength of ultra short waves, Radiotekhnika **12,** (1957). The quantity μ as used in his eq (28) is only valid if the antenna heights, h_1 and h_2, above the equivalent sphere are small compared to the radius. Clearly this is violated in Kalinin's application.

[23] K. Furutsu, Field strength in the vicinity of line of sight in diffraction, J. Radio Research Labs. (Tokyo) **3,** 55 (1956). (His functions $\chi_1^{(3)}$, $\chi_2^{(3)}$ etc. which are related to Airy integrals are usually approximated by the first term of their asymptotic expansions. It is difficult to see how this is justified near line of sight since the important values of z are not large in the "correction" terms. For example, in his eq (3.6) the leading term would vary as $\rho^{3/2}$ rather than $\rho^{1/2}$, if higher order terms of $\chi_1(z)$ and $\chi_2(z)$ are retained).

[24] T. T. Wu, The electromagnetic theory of light, Pt. I, Sci. Rept. No. 9, and T. T. Wu and S. R. Seshadri, Pt. II, Sci. Rept. No. 22, Cruft Lab., (Harvard Univ., 1958).

[25] J. B. Keller, Diffraction by a convex cylinder, IRE Trans. **AP–4,** 312 (1956).

[26] N. A. Logan, Fresnel diffraction by convex surfaces. Paper presented at Washington meeting of International Scientific Radio Union, May 4–7, 1959 (extensive numerical results for the care $q=0$ and ∞ and certain generalizations of the theory are reported in this paper).

Boulder, Colo. (Paper 63D2–17).